Published in final edited form as:

Cytoskeleton (Hoboken). 2018 February ; 75(2): 70–84. doi:10.1002/cm.21427.

Intraflagellar Transporter Protein 140 (IFT140), a component of IFT-A complex, is Essential for Male Fertility and Spermiogenesis in Mice

Yong Zhang[1,2], **Hong Liu**[2,3], **Wei Li**[2], **Zhengang Zhang**[2,4], **Shiyang Zhang**[2,3], **Maria E Teves**[2], **Courtney Stevens**[5], **James A Foster**[5], **Gregory E Campbell**[6], **Jolene J Windle**[6], **Rex A Hess**[7], **Gregory J Pazour**[8], and **Zhibing Zhang**[2,3]

[1]Department of Dermatology, Tongji Hospital, Tongji Medical College, Huazhong University of Science and Technology, Wuhan China, 430030

[2]Department of Obstetrics & Gynecology, Virginia Commonwealth University, Richmond, VA, 23298

[3]School of Public Health, Wuhan University of Science and Technology, Wuhan, Hubei, 430060

[4]Department of Gastroenterology, Tongji Hospital Affiliated to Tongji Medical College, Huazhong University of Science and Technology, Wuhan, Hubei, 430030

[5]Department of Biology, Randolph-Macon College, Ashland, VA 23005

[6]Department of Human and Molecular Genetics, Virginia Commonwealth University, Richmond, VA, 23298

[7]Department of Comparative Biosciences, College of Veterinary Medicine, University of Illinois, 2001 S. Lincoln, Urbana, IL 61802-6199

[8]Program in Molecular Medicine, University of Massachusetts Medical School, Worcester, MA 01605

Abstract

Intraflagellar transport (IFT) is a conserved mechanism essential for the assembly and maintenance of most eukaryotic cilia and flagella. However, little is known about its role in sperm flagella formation and male fertility. IFT140 is a component of IFT-A complex. In mouse, it is highly expressed in the testis. *Ift140* gene was inactivated specifically in mouse spermatocytes/spermatids. The mutant mice did not show any gross abnormalities, but all were infertile associated with significantly reduced sperm number and motility. Multiple sperm morphological abnormalities were discovered, including amorphous heads, short/bent flagella and swollen tail

Address correspondence to: Zhibing Zhang, MD, PhD, Associate Professor, Department of Obstetrics/Gynecology, Virginia Commonwealth University, 1101 E Marshall Street, Richmond, VA, 23298, zhibing.zhang@vcuhealth.org.

Competing interests

The authors have no conflict of interest.

Author contribution

Zhibing Zhang designed the experiments and wrote the paper. Y. Z., H. L., W. L., Zhengang Zhang, S. Y. Z., M. E. T., C. S., G. E. C and Zhibing Zhang performed the experiments. G. J. P. contributed reagents and materials. J. A.F., J. J. W., R. A. H., and Zhibing Zhang analyzed the data.

tips, as well as vesicles along the flagella due to spermiogenesis defects. The epididymides contained round bodies of cytoplasm derived from the sloughing of the cytoplasmic lobes and residual bodies. Knockout of *Ift140* did not significantly affect testicular expression levels of selective IFT components but localization of IFT27 and IFT88, two components of IFT-B complex was changed. Our findings demonstrate that IFT140 is a key regulator for male fertility and normal spermiogenesis in mice, it not only plays a role in sperm flagella assembling, but is also involved in critical assembly of proteins that interface between the germ cell plasma and the Sertoli cell.

Introduction

Cilia or flagella are evolutionarily conserved, microtubule-based cellular organelles that project from the cell surface. They are capable of sensing and transducing environmental signals and essential for cell motility (Satir and Christensen 2007). The assembly and maintenance of cilia/flagella are mediated by a motor-driven trafficking system termed intraflagellar transport (IFT), which was first described in the green algae *Chlamydomonas reinhardtii* (Ishikawa and Marshall 2011; Kozminski et al. 1993). IFT is characterized by a bidirectional movement of large protein complexes called IFT particles along the axoneme of cilia/flagella and functions independently of ciliary/flagellar beat (Kozminski et al. 1993; Prevo et al. 2017). IFT machinery is essential for the movement of IFT particles including ciliary/flagellar precursors and signaling molecules from the basal body to the site of assembly at the axonemal tip of cilia/flagella with the aid of kinesin-2 motors (anterograde trafficking) (Cole et al. 1998; Huet et al. 2014; Pedersen et al. 2006; Scholey 2013). The maintenance of cilia/flagella length is balanced by constant disassembly of microtubules at the tip, and thus the IFT system is required for cytoplasmic dynein 2-mediated transport of turnover products from the tip of an axoneme to the cell body (retrograde trafficking) (Pazour et al. 1999; Porter et al. 1999).

Study of IFT particles isolated from flagella of *C. reinhardtii* revealed that the IFT particles are composed of two complexes, IFT-A and IFT-B (Cole et al. 1998; Piperno and Mead 1997). The complex IFT-A contains 6 subunits while the complex IFT-B comprises 16 subunits. Many of these IFT proteins harbor typical protein-protein interaction domains including coiled-coil motifs, tetratricopeptide repeats (TPRs) or tryptophan/aspartic acid repeats (WD40 repeats) (Cole et al. 1998; Piperno and Mead 1997; Prevo et al. 2017). Mutations disrupting IFT subunits usually result in short or completely absent cilia/flagella, or formation of flagellar bulges due to defects in anterograde and/or retrograde transport (Absalon et al. 2008; Iomini et al. 2009; Tsao and Gorovsky 2008). In addition, knockdown of the IFT-A complex blocks access of Tubby-like protein 3 (TULP3) and G protein-coupled receptors into mammalian primary cilia (Hirano et al. 2017; Mukhopadhyay et al. 2010).

IFT140 belongs to the complex IFT-A and is conserved in green algae, mouse, fly, worm and human (Behal et al. 2012; Crouse et al. 2014; Jensen et al. 2010; Lee et al. 2008; Xu et al. 2015). By taking advantage of the yeast two-hybrid analysis, the organization of IFT-A has been proposed in which IFT140 is associated with IFT122 and IFT144 to a stable IFT-A core subcomplex (Behal et al. 2012). The composition of the IFT-A core has been confirmed by visible immunoprecipitation assays (Hirano et al. 2017). Depletion of IFT140 in

Trypanosoma brucei by RNAi led to accumulation of all IFT dynein proteins at the flagellar base and short flagella, which suggests that IFT140 is indispensable for entry of dynein proteins into the cytoplasm and flagellar assembly (Blisnick et al. 2014). Besides the involvement of assembly of chordotonal cilia, IFT140 is required for stable expression of TRPV calcium channel in *Drosophila* (Lee et al. 2008). Moreover, it has been reported that *Ift140* deficiency results in a broad spectrum of phenotypes associated with ciliopathies in mammals. In mouse, germline mutation of *Ift140* caused mid-gestation lethality of homozygotes (Caruana et al. 2013). Kidney collecting duct-specific deletion of mouse *Ift140* partially disrupted formation of primary cilia and caused cystic kidney (Jonassen et al. 2012). In humans, mutation of *Ift140* has been linked with Mainzer-Saldino syndrome and Jeune asphyxiating thoracic dystrophy, the rare disorder characterized by retinal dystrophy, chronic renal disease and skeletal abnormalities (Khan et al. 2014; Pena-Padilla et al. 2017; Perrault et al. 2012; Schmidts et al. 2013). The *Ift140* gene is also associated with non-syndromic retinal disorders including Leber congenital amaurosis and retinitis pigmentosa (Bayat et al. 2017; Xu et al. 2015), and IFT140 is required for development and maintenance of outer segments (Crouse et al. 2014).

Even though IFT140 is critical for ciliary/flagellar assembly and signal transduction, the requirement of IFT140 in spermatogenesis remains unclear. In the present study, we investigated the role of IFT140 in male germ cell development and male fertility. We discovered that mouse *Ift140* gene product is abundant in the testis, and the gene is up-regulated during spermiogenesis. The protein is present in the cytoplasm of round spermatids, and is translocated to the manchette of the elongating spermatids. Inactivation of the gene specifically in male germ cells gave rise to complete infertility associated with dramatically reduced sperm number and sperm motility. The few sperm passed through the full spermatogenesis process had short tails, distorted heads and disrupted sperm ultrastructure. Testicular expression levels of selected IFT proteins were not changed in the conditional *Ift140* mutant mice. However, localization of IFT27, a component of IFT-B component was changed. Our studies demonstrate that IFT140 is essential for sperm formation, in part through modulating other IFT molecules.

Results

IFT140 is abundantly expressed in the mouse testis

RT-PCR was performed using cDNA prepared from 9 mouse tissues to explore the tissue distribution and expression pattern of *Ift140. Ift140* mRNA was detected in most of these tissues with various expression levels, and was most highly expressed in the testis (Fig. 1A). Consistent with RT-PCR results, quantitative PCR analysis showed that expression of *Ift140* in the testis was much higher than that in the other tissues (Fig 1B). In addition, expression of IFT140 protein was examined by Western blot analysis. A 140 kDa IFT140 protein was detected exclusively in the testis (Fig. 1C). Testicular extracts were prepared from mice during the first wave of spermatogenesis, and expression of IFT140 was examined by Western blot analysis. IFT140 protein appeared to be expressed in a stage-specific manner; It was first observed at day 24 after birth and the protein level increased significantly

through day 30 and day 35 (Fig. 1D). The high level expression of IFT140 in the late stage of spermatogenesis suggests that IFT140 may play a role in spermiogenesis.

Generation of male germ cell-specific *Ift140* knockout mice

To study the function of IFT140 in spermatogenesis, we generated the conditional *Ift140* knockout mice using the *Cre/loxP* and *flp/FRT* system as described before (Zhang et al. 2016; Liu et al. 2017; Zhang et al. 2017). The homozygous KO mice were verified by PCR-based genotyping (Fig. S1). Since the *Ift140* gene was disrupted, it should be non-functional. As expected, Western blot analysis further confirmed that IFT140 was not detected in the KO mice (Fig. 2A). IFT140 expression in the germ cells was also examined by immunofluorescence staining. IFT140 was present in the cytoplasm of round spermatocytes and in the manchette of the elongating spermatids of the control mice (Fig. 2Ba, b). The signal was specific for IFT140 as no IFT140 protein was detected when the germ cells were incubated with pre-immune serum (Fig. S2). No specific IFT140 signal was detected in the germ cells isolated from conditional *Ift140* mutant mice. (Fig. 2Bc, d), indicating that the *Ift140* gene was disrupted in male germ cells.

IFT140 deficiency results in male infertility

To test the impact of inactivating of *Ift140* gene on male fertility, we bred control or *Ift140* knockout male mice (6 weeks old or mature) with 3 to 4 months old wild-type female mice for over 2 months. All the control males were fertile and produced offspring with normal litter size. Although the *Ift140* KO males showed normal sexual behavior and vaginal plugs were observed in the females, all these KO mice of the two age groups were sterile (Table 1).

Abnormal sperm, significantly reduced sperm count and motility in the conditional *Ift140* KO mice

To investigate the cause of infertility, cauda epididymal sperm were collected from the control and conditional *Ift140* knockout mice, and examined by light microscopy. The sperm density was remarkably higher in the control mice than that in the KO mice under the same dilution (Fig. S3). The control spermatozoa showed normal morphology whereas *Ift140* KO spermatozoa exhibited short and/or bent tails. Some sperm from mutant mice displayed vacuoles at the base of stunted flagella (Fig. 3Ab,c). More than 90% of the mutant sperm displayed no mobility and although the rest remained motile, the motility was significantly weaker than that of the control sperm. Most control sperm showed robust flagellar beating with forward motility while a small proportion of *Ift140*-null sperm exhibited low beating amplitude with limited forward movement (Fig. 3B–D, Supplementary Movies).

The developed sperm are stored in the cauda epididymides; therefore, histology of cauda epididymis of the control and the mutant mice was examined. The cauda epididymides of the control mice contained well-developed spermatozoa (Fig. 3E, left panel, Fig. S4, left two panels). However, in the *Ift140* KO mice, few sperm were found in the lumen of cauda epididymis (Fig. 3E, right three panels, Fig. S4, right two panels).

To further obtain insights into deformation of *Ift140* KO sperm, epididymal sperm from the mutant mice were examined by scanning electron microscopy (SEM). Sperm from the control mice had a condensed head with a long and smooth tail (Fig. 4a). However, the abnormal morphology of *Ift140* KO sperm, which have been observed under light microscopy, was better visualized by SEM. The sperm displayed amorphous heads, short/swollen flagella and other distorted shapes (Fig. 4b–f, Fig. S5).

To further examine the effect of germ cell-specific knockout of *Ift140* on sperm fertility, an in vitro fertilization assay was conducted. During the capacitation step of sperm collection, the control sperm efficiently swam to the periphery of the drop of incubation medium, while very few knockout sperm showed any motility. Following subsequent incubation of sperm from control and knockout males with C57BL/6J oocytes, the majority of oocytes incubated with control sperm developed normal polar bodies and pronuclei and progressed to the 2-cell stage, and almost all of those progressed to the 4-cell stage. In contrast, only 5 of 84 oocytes incubated with conditional *Ift140* knockout sperm progressed to the 2-cell stage, although 3 of these appeared distinctly abnormal, and none progressed to the 4-cell stage (data not shown).

Disruption of *Ift140* leads to defects in spermatogenesis

Since spermatogenesis occurs in the seminiferous tubules of the testis, histology of testes of the control and *Ift140* KO mice was examined. Testis size of the mutant mice appeared to be normal, and there was no significant difference in the testis weight and testis/body weight between the control and the KO mice (Fig. S6). H&E staining demonstrated normal seminiferous tubule architecture in the control mice, and the lumen was filled with spermatozoa (Fig. 5a–c, Fig. S7; left two panels). However, in the *Ift140* KO mice testes, spermatogenesis appeared normal through meiotic division and the early steps of spermiogenesis, although flagella in the early round spermatids were not observed extending into the lumen. Abnormal spermatogenesis was observed in the final phase, spermiogenesis. Abnormal shapes of the developing spermatid heads began to appear in stage X. The reduction of sperm numbers in the cauda epididymis was due to failure of spermiation, as step 16 spermatids were observed phagocytosed along the basement membrane after stage VIII (Fig. 5d–j). The lumen contained degenerated cells and few sperm. Occasionally some sperm could be found, but they had short tails and developing flagella were rarely observed in the lumen (Fig. 5e, f, I, j; Fig. S7, right two panels).

Abnormal epididymal and testicular sperm ultrastructure examined by TEM

To examine the sperm ultrastructure of the conditional *Ift140* knockout mice, TEM was conducted in both epididymal and testicular sperm. Epididymal sperm from the control mice showed normal “9+2” motile cilia axoneme structure, and accessory structures were also normally organized (Fig. 6a). Very few sperm were discovered in the conditional knockout preparations, and multiple abnormalities were discovered in almost all epididymal sperm recovered from the conditional *Ift140* KO mice, including disorganized axoneme microtubule array, mis-placed ODFs, fibrous sheath and mitochondria components, disrupted “9+2” core axoneme structure and abnormal chromatin (Fig. 6b–j, Fig. S8a–h).

Some sperm with apparently normal ultrastructure in cross-sections were still observed in the conditional Ift140 KO mice (Fig. 6e, f, h).

Ultrastructure of the testicular sperm was also examined. In the control mice, similar to the epididymal sperm, TEM revealed normal core axoneme and accessory structure of testicular sperm (Fig. 7a, b). Very few axoneme structures could be seen in the seminiferous tubules from the *Ift140* KO mice (Fig. 7c). From the images of the few developed sperm, none showed normal morphology. The same defects as seen in the epididymal sperm were observed (Fig. 7c–h, and Fig. S9a–h).

Effect of IFT140 deficiency on expression of other IFT proteins

It has been reported that IFT proteins are capable of forming complexes with other IFT proteins in order to transport ciliary components for normal ciliogenesis (Ishikawa and Marshall 2011). To study the potential functional association between IFT140 and other IFT proteins, the effect of *Ift140* disruption on expression of selective IFT proteins was examined by Western blot analysis. The protein level of IFT20, IFT25, IFT27, IFT74, IFT81 and IFT88 in the control mice remained similar to the *Ift140* KO mice (Fig. 8A). Consistently, quantitative analysis indicated that there was no significant difference in the expression of these IFT proteins between the control and *Ift140* KO mice (Fig. 8B). Localization of selective IFT proteins, including IFT20, IFT27 and IFT88, was examined in the conditional *Ift140* knockout mice. As reported previously, IFT20 was present in the Golgi bodies in the spermatocytes, the acrosome in round spermatids, and manchette of elongating spermatids (Fig. 8C, upper three panels). IFT20 localization was not significantly changed in the *Ift140* knockout mice, except that in round spermatids, IFT20 does not seem to attach closely to the nuclear membrane (Fig. 8C, lower three panels). IFT27 protein was present throughout the cytoplasm of round spermatids of the control mice. However, in the absence of IFT140, it appeared to form a large vesicle, which was never seen in the germ cells from the control mice (Fig. 8D). In the control mice, IFT88 was present in the cytoplasm of spermatocytes and round spermatids, as well as the manchette of elongating spermatids and the developing tail. However, in the conditional *Ift140* mice, even though IFT88 was still present in the cytoplasm of spermatocytes and round spermatids, it was absence from the manchette of elongating spermatids, and the protein showed abnormal accumulation in the cells at later stages (Fig. 8E).

Discussion

Cilia and flagella are microtubule-based cellular structures that play critical roles in cell motility as well as sensing and processing extracellular stimuli through various signal transduction pathways such as the Hedgehog and Wnt pathways (Mourao et al. 2016; Singla and Reiter 2006). The formation and maintenance of cilia/flagella are primarily mediated by the IFT system (Prevo et al. 2017). IFT140 is a core component of the IFT-A complex and is essential for cargo transport for ciliary/flagellar assembly. Disruption of *Ift140* in *Chlamydomonas* and *Trypanosoma* resulted in formation of short flagella (Absalon et al. 2008; Zhu et al. 2017). In addition, IFT140 has been reported to associate with early embryonic development in mouse and human ciliopathies (Caruana et al. 2013; Khan et al.

2014; Perrault et al. 2012; Schmidts et al. 2013; Xu et al. 2015). However, the function of IFT proteins in the assembly of mammalian sperm flagella is poorly understood.

In the present study, the high expression level of *Ift140* in the mouse testis suggests it is involved in the formation of sperm flagella. As global knockout of IFT proteins is lethal to embryo development (Keady et al. 2011; Marszalek et al. 1999; Nonaka et al. 1998), we generated male germ cell-specific *Ift140* knockout mice and found that IFT140 is required for spermatogenesis. In conditional *Ift140* mutant mice, only a few sperm were collected in cauda epididymis, and were abnormal in appearance, as well as defective in cell motility. The abnormalities of sperm production and motility would account for the male infertility. None of conditional *Ift140* KO mice produced offspring and all the males were infertile. In vitro fertilization assay further supported that IFT140 plays a critical role in normal sperm function and male fertility.

Immunofluorescence staining on the isolated germ cells showed that IFT140 is localized in the cytoplasm of round spermatids. However, in the elongating spermatids, it is highly abundant in the manchette, a transient unique structure only present in the male germ cells (Lehti and Sironen 2016). The manchette is enriched in microtubules and is believed to transport cargo proteins for sperm flagellum formation through the intra-manchette mechanism (IMT) (Kierszenbaum 2002). IMT is different from IFT because IMT is a transient structure inside the cell bodies of the elongating spermatids while IFT is within the developing cilia/flagella. However, the two processes share many common features in that both use motor proteins for cargo transport (Taschner and Lorentzen 2016; Kierszenbaum 2002). IFT140 is present in the manchette, suggesting that the protein might be involved in the IMT process. Without IFT140, the IMT process might be affected, and cargo proteins are not delivered to the basal bodies for the next IFT process, and thus spermiogenesis is disrupted. Our staining of control mice did not reveal IFT140 localization in the developing flagella, it is likely that the antibody is not sensitive enough to probe the IFT140 protein in the developing sperm flagellum.

Under light microscopy and SEM, the few IFT140 knockout sperm that were transported to the cauda epididymis displayed abnormal morphologies including bulged flagellar tips (Fig. 3 4), which are typical phenotypes of retrograde trafficking deficiency (Hirano et al. 2017; Iomini et al. 2009; Tsao and Gorovsky 2008). This observation suggests IFT140 is involved in retrograde transport of flagellar components and is consistent with disruption of specific retrograde IFT proteins in *Tetrahymena*, *Chlamydomonas* and nematode (Blacque et al. 2006; Iomini et al. 2009; Tsao and Gorovsky 2008). However, defects in retrograde transport only can't explain other phenotypes discovered in the knockout mice, for example, the short tails, and redundant cytoplasm in the sperm; thus, other mechanisms must exist. In *Trypanosoma brucei,* IFT140 is essential for localization of IFT-dynein motors from the cytoplasmic pool to the base of flagella (Blisnick et al. 2014), a likely IMT function in male germ cells. The presence of flagellar bulges in the *Ift140* KO mice may result from lack of the IFT-dynein motors that drive retrograde transport and thus lead to accumulation of axonemal turnover products in the sperm flagella, as well as other proteins which could lead to excessive accumulation of cytoplasm in the elongating spermatids, as observed beginning in stage XII.

Our laboratory has generated germ cell-specific *Ift20, Ift25* and *Ift27* knockout mice (Liu et al. 2017; Zhang et al. 2016; Zhang et al. 2017). Conditional IFT140 knockout mice shared some similarities to these mutant mice. Similar to the conditional *Ift20* KO mice, significant amount of cytoplasmic residual bodies and sperm with redundant cytoplasm were discovered in the conditional *Ift140* KO epididymides, but these were not seen in the conditional *Ift25* and *Ift27* mutant mice. As discussed previously, this phenomenon might be caused by a defect in Sertoli/germ cell recognition and failure of residual body formation and Sertoli cell phagocytosis of the excess germ cell cytoplasm (Wen et al. 2016). Even though IFT20 and IFT140 are reported to be present in different IFT complexes in *Chlamydomonas*, with IFT20 in IFT-B complex, and IFT140 in IFT-A complex. The two IFT components may coordinate to remove redundant cytoplasm in male germ cells. IFT20 deficient mice were also sterile due to defects in the assembly and function of sperm flagella (Zhang et al. 2016). Both *Ift20* and *Ift140*-deficient sperms displayed short or loss of flagella and round heads, suggesting that IFT140 may also be implicated in anterograde transport of flagella precursors even though it is a component of the IFT-A complex. Indeed, the IFT-A complex is believed to function in anterograde trafficking as it links kinesin-2 to the IFT cargo for formation of the middle segment in *C. elegans* sensory cilia (Ou et al. 2007; Snow et al. 2004). In *Chlamydomonas*, loss of *ift140* affects the integrity and stability of the IFT-A complex that are crucial for moving flagellar precursors from the cytoplasmic compartment to the basal body for flagellar assembly (Zhu et al. 2017). The similar effect of IFT140 on the IFT-A complex may also contribute to the abnormal sperm morphology in mouse. Moreover, TEM of testicular and epididymal sperm from both *Ift20* and *Ift140*-deficient mice revealed similar abnormal sperm ultrastructure including deformed chromatin, disrupted “9+2” axoneme structure, increased numbers of residual bodies and retained cytoplasm (Zhang et al. 2016). It has been reported that IFT20 may play an important role in regulation of autophagy during spermiogenesis, a developmental process required for degradation of dysfunctional or unnecessary cytoplasmic contents via lysosomes (Kobayashi 2015; Zhang et al. 2016). The similar abnormal morphologies between *Ift140* and *Ift20*-deficient sperm imply that IFT140 might be implicated in autophagy process in spermatogenesis. However, as disruption of *Ift140* in mice did not impact on the expression of *Ift20*, it is likely that IFT140 functions independent of IFT20 and they might exert effects through different mechanisms.

IFT25 directly binds IFT27 (Liu et al. 2017). The two IFT proteins are not required for ciliogenesis in somatic cells (Eguether et al. 2014; Yang et al. 2015); however, both play essential roles in sperm formation and function (Liu et al. 2017; Wen et al. 2016; Zhang et al. 2017). Residual bodies and redundant sperm cytoplasm were not present in the preparation of the two conditional knockout mice, suggesting that IFT140 has a different role compared to the two IFT molecules. In addition, the striking phenotypes discovered in the two mutant mice were disrupted accessory structures that result in sperm immotility. Many developed sperm appear to have normal length, which is also different from the *Ift140* knockout mice, in which the developed sperm have significantly reduced sperm length. It is interesting, localization of IFT27 is disrupted in the *Ift140* knockout mice, suggesting that the two IFT proteins are functionally related. Similar to IFT27, localization of IFT88, another IFT-B complex component also essential for male fertility and sperm flagella

formation, was also disrupted in the germ cells at late stage of *Ift140* knockout mice (San Augustin et al. 2015). It is possible that IFT140 is an upstream protein of IFT27 and IFT88 and is responsible for carrying the two IFT proteins in the male germ cells. Interestingly, localization of IFT20 was not changed significantly in the conditional *Ift140* KO mice, even though it appeared that in the round spermatids, IFT20 attached to the nuclear membrane more closely. Different change in localization of these IFT proteins in the conditional *Ift140* KO mice strongly suggests that IFT140 has a different correlation with other IFT proteins in male germ cells.

In summary, we studied the function of IFT140 in mouse sperm development and demonstrated that this protein is required for the completion of spermatogenesis. IFT140 mediates the formation of sperm flagella though transporting essential proteins including sperm structural proteins and other IFT components, and probably helping to position excess cytoplasm and essential proteins involved in the formation of the cytoplasmic lobe and phagocytosis of the residual body at the end of spermiogenesis.

Materials and Methods

Ethics Statement

All animal studies were approved by Virginia Commonwealth University Institutional Animal Care and Use Program Advisory Committee (Protocol number: AD10000167).

RT-PCR and real-time PCR

Total RNA was extracted from mouse tissues using TRIzol™ reagent (Invitrogen) and reversed transcribed to cDNA using RevertAid first strand cDNA synthesis kit (ThermoFisher). cDNA was used for RT-PCR or real-time PCR to examine *Ift140* mRNA expression with the following primers: forward:5′-TCCGTATTCACTGCTTCCAG-3′; and reverse:5′-AGTCTCCAGTCTCGTTGGCT-3′. Real-time PCR was performed using iTaq™ Universal SYBR® Green Supermix. *Gapdh* was used to normalize the expression level of *Ift140*.

Western blot analysis

Western blotting was performed as previously described (Liu et al. 2017). The membranes were immunoblotted with indicated antibodies at 4°C overnight: anti-IFT140, anti-IFT88, anti-IFT20 and anti-IFT27 (1:2000, Dr. Pazour's laboratory); anti-IFT25 (1:2000, Protein Tech, 15732-1-AP); anti-IFT74 (1:1000, Antibody Verify); anti-IFT81 (1:1000, Proteintech Group); anti-β-actin (1:2000, Cell Signaling). After washing, the membrane was incubated with the secondary antibody conjugated with horseradish peroxidase (1:2000). Signals were detected with SuperSignal™ West Pico Chemiluminescent Substrate and West Femto Maximum Sensitivity Substrate (ThermoFisher).

Generation of male germ cell-specific *Ift140* knockout mice

Stra8-iCre mice were purchased from Jackson Laboratory (Stock No: 008208). Transgenic mouse line *Stra8-cre* expresses improved Cre recombinase under the control of a 1.4 Kb promoter region of the germ cell-specific stimulated by retinoic acid gene 8 (*Stra8*) (Sadate-

Ngatchou et al. 2008). *If140*$^{flox/flox}$ mice were generated by Dr. Gregory J. Pazour, University of Massachusetts Medical School (Eguether et al. 2014). To generate germ cell specific *Ift140* knockout mice, we followed the same breeding strategy as to generate germ cell specific *Ift20* and *Ift25* knockout mice (Liu et al. 2017; Zhang et al. 2016). Briefly, three to four-month old *Stra8-cre* males were crossed with three to four-month old *Ift140*$^{flox/flox}$ females to obtain *Stra8-iCre; Ift140*$^{flox/+}$ mice. The three to four-month old *Stra8-iCre; Ift140*$^{flox/+}$ males were crossed back with three- to four-month old *Ift140*$^{flox/flox}$ females again, and the *Stra8-iCre; Ift140*$^{flox/flox}$ were considered to be the homozygous knockout mice (KO), and *Stra8-iCre; Ift140*$^{flox/+}$ mice were used as the controls. Mice were genotyped by PCR using multiplex PCR mix (Bioline, Cat No BIO25043). The presence of the *Stra8-iCre* allele was evaluated as described in (Sadate-Ngatchou et al. 2008), and *Ift*140 genotypes were determined as described previously (Eguether et al. 2014).

Assessment of fertility and fecundity

To assess fertility and fecundity, 6-week old or adult *Ift140* KO (*Stra8-iCre; Ift140*$^{flox/flox}$) and control (*Stra8-iCre; Ift140*$^{flox/+}$) males were paired with 3–4 months old wild-type females for at least 2 months. The number of pregnant mice and the number of offspring from each pregnancy were recorded.

Spermatozoa counting

Sperm were collected from cauda epididymides and fixed in 2% formaldehyde for 10 minutes at room temperature. After washing and re-suspending in PBS buffer, sperm were counted using a hemocytometer chamber under a light microscope. The number of sperm was calculated as previously described (Zhang et al. 2006).

Spermatozoa motility assay

Assessment of sperm motility was carried out following a previously described procedure (Liu et al. 2017). Movies were taken at 30 frames/sec. For each sperm sample, ten fields were analyzed.

Histological staining on tissues

Mouse testes and epididymides were prepared for histological analysis using previously described methods (Liu et al. 2017). Briefly, samples were fixed in PBS buffer containing 4% formaldehyde, sectioned into 5 μm slides and stained with hematoxylin and eosin.

Isolation of spermatogenic cells and immunofluorescence (IF) analysis

Testes from adult mice were dissected in a petri dish with 5 mL DMEM containing 0.5 mg/mL collagenase IV and 1.0 μg/mL DNAse I (Sigma-Aldrich), and was incubated for 30 min at 32°C with gentle stirring, released spermatogenic cells were pelleted by centrifugation (5 min at 1000 rpm, 4°C). After washing with PBS, the cells were fixed with 5ml of 4% paraformaldehyde (PFA) containing 0.1 M sucrose at room temperature. The dispersed, mixed testicular cells were washed three times with PBS. Afterwards, the cells were re-suspended in 2 ml of warm PBS and 50 μl of cell suspension was loaded to the slide and allowed to air-dry. Cells were permeabilized with 0.1 % Triton X-100 (Sigma-Aldrich)

for 5 min at 37°C, washed with PBS three times, and blocked with 10 % goat serum in PBS for 1 hr. Then cells were washed three times with PBS and incubated overnight with the indicated primary antibodies. After extensive wash with PBS, the cells were incubated with Cy3-conjugated anti-rabbit IgG secondary antibody for 1 hr. The slides were washed with PBS and mounted in VectaMount with DAPI (Vector Labs. Burlin-game, CA) and sealed with nail polish. Images were captured by confocal laser-scanning microscopy as before.

Scanning electron microscopy (SEM)

Cauda epididymal sperm were collected and fixed in 0.1M sodium cacodylate buffer containing 3% glutaraldehyde and 1% paraformaldehyde (pH7.4) at 4°C overnight and processed using standard methods (Liu et al. 2017).

Transmission electron microscopy (TEM)

Mouse testes and cauda epididymal sperm were fixed in the same buffer as scanning electron microscopy. Images were taken with a Hitachi HT7700 transmission electron microscope.

In vitro fertilization assay (IVF)

To examine the effect of germ cell-specific knockout of *Ift140* on sperm fertility, we performed an in vitro fertilization assay using sperm isolated from control and conditional *Ift140* knockout mice using the method described by the Nakagata laboratory (http://card.medic.kumamoto-u.ac.jp/card/english/sigen/manual/onlinemanual.html).

Supplementary Material

Refer to Web version on PubMed Central for supplementary material.

Acknowledgments

We thank Dr. Scott C. Henderson, and Judy C. Williamson for their assistance with using the electronic microscopy in Microscopy Core Facility of Virginia Commonwealth University.

Funding

This research was supported by NIH grant HD076257, HD090306, Virginia Commonwealth University Presidential Research Incentive Program (PRIP) and Massey Cancer Award (to ZZ), NIH grant GM060992 (to GJP), Chenery and Rashkind Grants from Randolph-Macon College (JF). Natural Science Foundation of China (81571428, 81370750), and Special Fund of Wuhan University of Science and Technology for Master Student's short-term studying abroad. Confocal microscopy and SEM were performed in the VCU Microscopy Facility of Virginia Commonwealth University (5P30NS047463). TEM was performed at Randolph-Macon College (NSF1229184).

Services in support of the IVF project were provided by the VCU Massey Cancer Center. Transgenic/Knockout Mouse Core, supported in part with funding from NIH-NCI Cancer Center Support Grant P30 CA016059.

References

Absalon S, Blisnick T, Kohl L, Toutirais G, Dore G, Julkowska D, Tavenet A, Bastin P. Intraflagellar transport and functional analysis of genes required for flagellum formation in trypanosomes. Mol Biol Cell. 2008; 19(3):929–44. [PubMed: 18094047]

Bayat A, Kerr B, Douzgou S. Study DDD. The evolving craniofacial phenotype of a patient with Sensenbrenner syndrome caused by IFT140 compound heterozygous mutations. Clin Dysmorphol. 2017

Behal RH, Miller MS, Qin H, Lucker BF, Jones A, Cole DG. Subunit interactions and organization of the Chlamydomonas reinhardtii intraflagellar transport complex A proteins. J Biol Chem. 2012; 287(15):11689–703. [PubMed: 22170070]

Blacque OE, Li C, Inglis PN, Esmail MA, Ou G, Mah AK, Baillie DL, Scholey JM, Leroux MR. The WD repeat-containing protein IFTA-1 is required for retrograde intraflagellar transport. Mol Biol Cell. 2006; 17(12):5053–62. [PubMed: 17021254]

Blisnick T, Buisson J, Absalon S, Marie A, Cayet N, Bastin P. The intraflagellar transport dynein complex of trypanosomes is made of a heterodimer of dynein heavy chains and of light and intermediate chains of distinct functions. Mol Biol Cell. 2014; 25(17):2620–33. [PubMed: 24989795]

Caruana G, Farlie PG, Hart AH, Bagheri-Fam S, Wallace MJ, Dobbie MS, Gordon CT, Miller KA, Whittle B, Abud HE, et al. Genome-wide ENU mutagenesis in combination with high density SNP analysis and exome sequencing provides rapid identification of novel mouse models of developmental disease. PLoS One. 2013; 8(3):e55429. [PubMed: 23469164]

Cole DG, Diener DR, Himelblau AL, Beech PL, Fuster JC, Rosenbaum JL. Chlamydomonas kinesin-II-dependent intraflagellar transport (IFT): IFT particles contain proteins required for ciliary assembly in Caenorhabditis elegans sensory neurons. J Cell Biol. 1998; 141(4):993–1008. [PubMed: 9585417]

Crouse JA, Lopes VS, Sanagustin JT, Keady BT, Williams DS, Pazour GJ. Distinct functions for IFT140 and IFT20 in opsin transport. Cytoskeleton (Hoboken). 2014; 71(5):302–10. [PubMed: 24619649]

Eguether T, San Agustin JT, Keady BT, Jonassen JA, Liang Y, Francis R, Tobita K, Johnson CA, Abdelhamed ZA, Lo CW, et al. IFT27 links the BBSome to IFT for maintenance of the ciliary signaling compartment. Dev Cell. 2014; 31(3):279–90. [PubMed: 25446516]

Hirano T, Katoh Y, Nakayama K. Intraflagellar transport-A complex mediates ciliary entry and retrograde trafficking of ciliary G protein-coupled receptors. Mol Biol Cell. 2017; 28(3):429–439. [PubMed: 27932497]

Huet D, Blisnick T, Perrot S, Bastin P. The GTPase IFT27 is involved in both anterograde and retrograde intraflagellar transport. Elife. 2014; 3:e02419. [PubMed: 24843028]

Iomini C, Li L, Esparza JM, Dutcher SK. Retrograde intraflagellar transport mutants identify complex A proteins with multiple genetic interactions in Chlamydomonas reinhardtii. Genetics. 2009; 183(3):885–96. [PubMed: 19720863]

Ishikawa H, Marshall WF. Ciliogenesis: building the cell's antenna. Nat Rev Mol Cell Biol. 2011; 12(4):222–34. [PubMed: 21427764]

Jensen VL, Bialas NJ, Bishop-Hurley SL, Molday LL, Kida K, Nguyen PA, Blacque OE, Molday RS, Leroux MR, Riddle DL. Localization of a guanylyl cyclase to chemosensory cilia requires the novel ciliary MYND domain protein DAF-25. PLoS Genet. 2010; 6(11):e1001199. [PubMed: 21124868]

Jonassen JA, SanAgustin J, Baker SP, Pazour GJ. Disruption of IFT complex A causes cystic kidneys without mitotic spindle misorientation. J Am Soc Nephrol. 2012; 23(4):641–51. [PubMed: 22282595]

Keady BT, Le YZ, Pazour GJ. IFT20 is required for opsin trafficking and photoreceptor outer segment development. Mol Biol Cell. 2011; 22(7):921–30. [PubMed: 21307337]

Khan AO, Bolz HJ, Bergmann C. Early-onset severe retinal dystrophy as the initial presentation of IFT140-related skeletal ciliopathy. J AAPOS. 2014; 18(2):203–5. [PubMed: 24698627]

Kierszenbaum AL. Intramanchette transport (IMT): managing the making of the spermatid head, centrosome, and tail. Mol Reprod Dev. 2002; 63(1):1–4. [PubMed: 12211054]

Kobayashi S. Choose Delicately and Reuse Adequately: The Newly Revealed Process of Autophagy. Biol Pharm Bull. 2015; 38(8):1098–103. [PubMed: 26235572]

Kozminski KG, Johnson KA, Forscher P, Rosenbaum JL. A motility in the eukaryotic flagellum unrelated to flagellar beating. Proc Natl Acad Sci U S A. 1993; 90(12):5519–23. [PubMed: 8516294]

Lehti MS, Sironen A. Formation and function of the manchette and flagellum during spermatogenesis. Reproduction. 2016; 151(4):R43–54. [PubMed: 26792866]

Liu H, Li W, Zhang Y, Zhang Z, Shang X, Zhang L, Zhang S, Li Y, Somoza AV, Delpi B, et al. IFT25, an intraflagellar transporter protein dispensable for ciliogenesis in somatic cells, is essential for sperm flagella formation. Biol Reprod. 2017

Marszalek JR, Ruiz-Lozano P, Roberts E, Chien KR, Goldstein LS. Situs inversus and embryonic ciliary morphogenesis defects in mouse mutants lacking the KIF3A subunit of kinesin-II. Proc Natl Acad Sci U S A. 1999; 96(9):5043–8. [PubMed: 10220415]

Mourao A, Christensen ST, Lorentzen E. The intraflagellar transport machinery in ciliary signaling. Curr Opin Struct Biol. 2016; 41:98–108. [PubMed: 27393972]

Mukhopadhyay S, Wen X, Chih B, Nelson CD, Lane WS, Scales SJ, Jackson PK. TULP3 bridges the IFT-A complex and membrane phosphoinositides to promote trafficking of G protein-coupled receptors into primary cilia. Genes Dev. 2010; 24(19):2180–93. [PubMed: 20889716]

Nonaka S, Tanaka Y, Okada Y, Takeda S, Harada A, Kanai Y, Kido M, Hirokawa N. Randomization of left-right asymmetry due to loss of nodal cilia generating leftward flow of extraembryonic fluid in mice lacking KIF3B motor protein. Cell. 1998; 95(6):829–37. [PubMed: 9865700]

Ou G, Koga M, Blacque OE, Murayama T, Ohshima Y, Schafer JC, Li C, Yoder BK, Leroux MR, Scholey JM. Sensory Ciliogenesis in Caenorhabditis elegans: Assignment of IFT Components into Distinct Modules Based on Transport and Phenotypic Profiles. Molecular Biology of the Cell. 2007; 18(5):1554–1569. [PubMed: 17314406]

Pazour GJ, Dickert BL, Witman GB. The DHC1b (DHC2) isoform of cytoplasmic dynein is required for flagellar assembly. J Cell Biol. 1999; 144(3):473–81. [PubMed: 9971742]

Pedersen LB, Geimer S, Rosenbaum JL. Dissecting the molecular mechanisms of intraflagellar transport in chlamydomonas. Curr Biol. 2006; 16(5):450–9. [PubMed: 16527740]

Pena-Padilla C, Marshall CR, Walker S, Scherer SW, Tavares-Macias G, Razo-Jimenez G, Bobadilla-Morales L, Acosta-Fernandez E, Corona-Rivera A, Mendoza-Londono R, et al. Compound heterozygous mutations in the IFT140 gene cause Opitz trigonocephaly C syndrome in a patient with typical features of a ciliopathy. Clin Genet. 2017; 91(4):640–646. [PubMed: 27874174]

Perrault I, Saunier S, Hanein S, Filhol E, Bizet AA, Collins F, Salih MA, Gerber S, Delphin N, Bigot K, et al. Mainzer-Saldino syndrome is a ciliopathy caused by IFT140 mutations. Am J Hum Genet. 2012; 90(5):864–70. [PubMed: 22503633]

Piperno G, Mead K. Transport of a novel complex in the cytoplasmic matrix of Chlamydomonas flagella. Proc Natl Acad Sci U S A. 1997; 94(9):4457–62. [PubMed: 9114011]

Porter ME, Bower R, Knott JA, Byrd P, Dentler W. Cytoplasmic dynein heavy chain 1b is required for flagellar assembly in Chlamydomonas. Mol Biol Cell. 1999; 10(3):693–712. [PubMed: 10069812]

Prevo B, Scholey JM, Peterman EJG. Intraflagellar transport: mechanisms of motor action, cooperation, and cargo delivery. FEBS J. 2017

Sadate-Ngatchou PI, Payne CJ, Dearth AT, Braun RE. Cre recombinase activity specific to postnatal, premeiotic male germ cells in transgenic mice. Genesis. 2008; 46(12):738–42. [PubMed: 18850594]

San Agustin JT, Pazour GJ, Witman GB. Intraflagellar transport is essential for mammalian spermiogenesis but is absent in mature sperm. Mol Biol Cell. 2015; 26(24):4358–72. [PubMed: 26424803]

Satir P, Christensen ST. Overview of structure and function of mammalian cilia. Annu Rev Physiol. 2007; 69:377–400. [PubMed: 17009929]

Schmidts M, Frank V, Eisenberger T, Al Turki S, Bizet AA, Antony D, Rix S, Decker C, Bachmann N, Bald M, et al. Combined NGS approaches identify mutations in the intraflagellar transport gene IFT140 in skeletal ciliopathies with early progressive kidney Disease. Hum Mutat. 2013; 34(5): 714–24. [PubMed: 23418020]

Scholey JM. Kinesin-2: a family of heterotrimeric and homodimeric motors with diverse intracellular transport functions. Annu Rev Cell Dev Biol. 2013; 29:443–69. [PubMed: 23750925]

Singla V, Reiter JF. The primary cilium as the cell's antenna: signaling at a sensory organelle. Science. 2006; 313(5787):629–33. [PubMed: 16888132]

Snow JJ, Ou G, Gunnarson AL, Walker MRS, Zhou HM, Brust-Mascher I, Scholey JM. Two anterograde intraflagellar transport motors cooperate to build sensory cilia on C. elegans neurons. Nat Cell Biol. 2004; 6(11):1109–1113. [PubMed: 15489852]

Taschner M, Lorentzen E. The Intraflagellar Transport Machinery. Cold Spring Harb Perspect Biol. 2016; 8(10)

Tsao CC, Gorovsky MA. Tetrahymena IFT122A is not essential for cilia assembly but plays a role in returning IFT proteins from the ciliary tip to the cell body. J Cell Sci. 2008; 121(Pt 4):428–36. [PubMed: 18211962]

Wen Q, Tang EI, Xiao X, Gao Y, Chu DS, Mruk DD, Silvestrini B, Cheng CY. Transport of germ cells across the seminiferous epithelium during spermatogenesis-the involvement of both actin- and microtubule-based cytoskeletons. Tissue Barriers. 2016; 4(4):e1265042. [PubMed: 28123928]

Xu M, Yang L, Wang F, Li H, Wang X, Wang W, Ge Z, Wang K, Zhao L, Li H, et al. Mutations in human IFT140 cause non-syndromic retinal degeneration. Hum Genet. 2015; 134(10):1069–78. [PubMed: 26216056]

Yang N, Li L, Eguether T, Sundberg JP, Pazour GJ, Chen J. Intraflagellar transport 27 is essential for hedgehog signaling but dispensable for ciliogenesis during hair follicle morphogenesis. Development. 2015; 142(12):2194–202. [PubMed: 26023097]

Zhang Z, Kostetskii I, Tang W, Haig-Ladewig L, Sapiro R, Wei Z, Patel AM, Bennett J, Gerton GL, Moss SB, et al. Deficiency of SPAG16L causes male infertility associated with impaired sperm motility. Biol Reprod. 2006; 74(4):751–9. [PubMed: 16382026]

Zhang Z, Li W, Zhang Y, Zhang L, Teves ME, Liu H, Strauss JF 3rd, Pazour GJ, Foster JA, Hess RA, et al. Intraflagellar transport protein IFT20 is essential for male fertility and spermiogenesis in mice. Mol Biol Cell. 2016

Zhang Y, Liu H, Li W, Zhang Z, Shang X, Zhang D, Li Y, Zhang S, Liu J, Hess RA, et al. Intraflagellar Transporter Protein (IFT27), an IFT25 binding pertner, Is Essential For Male Fertility and Spermiogenesis In Mice. Dev Biol. 2017

Zhu B, Zhu X, Wang L, Liang Y, Feng Q, Pan J. Functional exploration of the IFT-A complex in intraflagellar transport and ciliogenesis. PLoS Genet. 2017; 13(2):e1006627. [PubMed: 28207750]

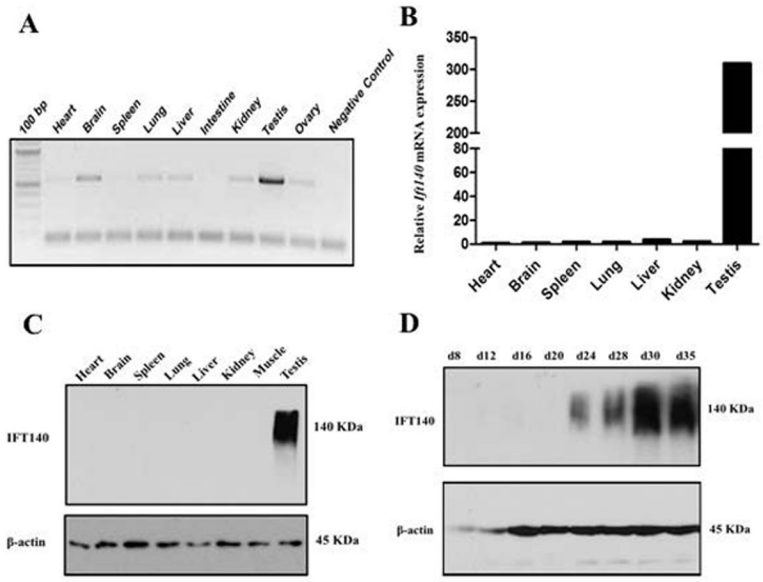

Figure 1. IFT140 is highly expressed in the testis and the protein level is elevated during spermiogenesis

A. Analysis of *Ift140* mRNA tissue distribution of by RT-PCR. *Ift140* mRNA is detected in most tissues, but is abundant only in the testis; B. Measurement of relative *Ift140* mRNA expression levels in mouse tissues by quantitative PCR. Expression levels were normalized to *Gapdh*. C. IFT140 protein expression in mouse tissues. Notice that IFT140 was detected only in the testis. D. Testicular IFT140 expression during the first wave of spermatogenesis. Notice that it was expressed at day 24 after birth and up-regulated afterwards, when germ cells enter spermiogenesis phase.

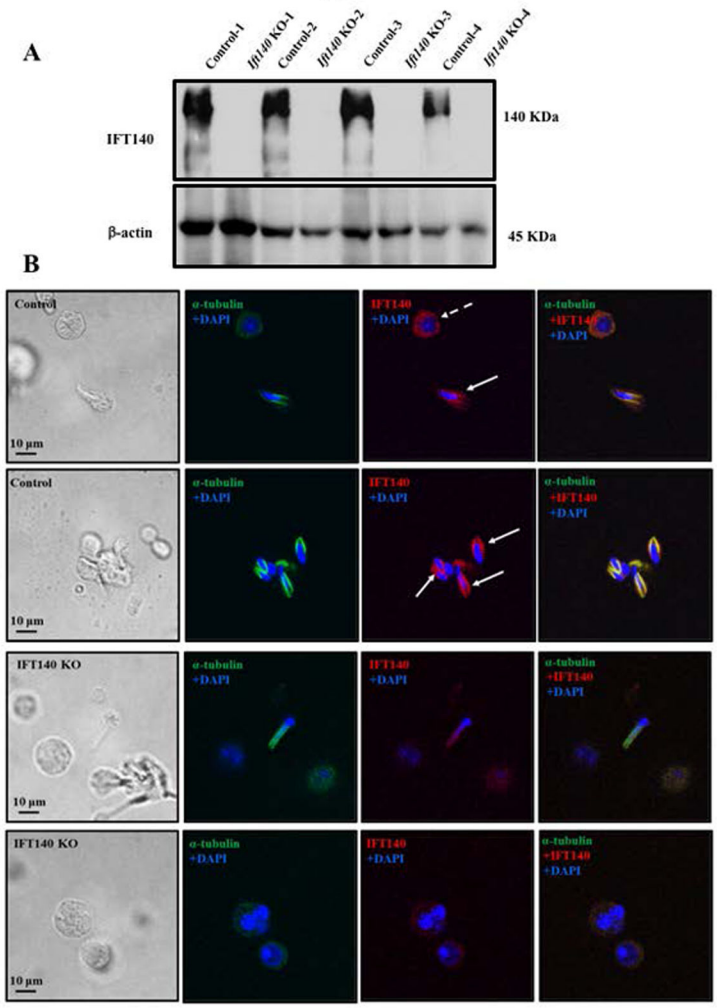

Figure 2. IFT140 protein expression in the control and conditional *Ift140* knockout mice

A. Western blot analysis of testicular IFT140 expression. IFT140 was detected in four control mice whereas it was absent in four KO mice. B. Examination of IFT140 expression and localization in isolated germ cells by immunofluorescence staining. IFT140 signal was observed in the cytoplasm of round spermatids and (dashed arrow) the manchette of the elongating spermatids (arrows) of the control mice, but the signal was not detected in the KO mice.

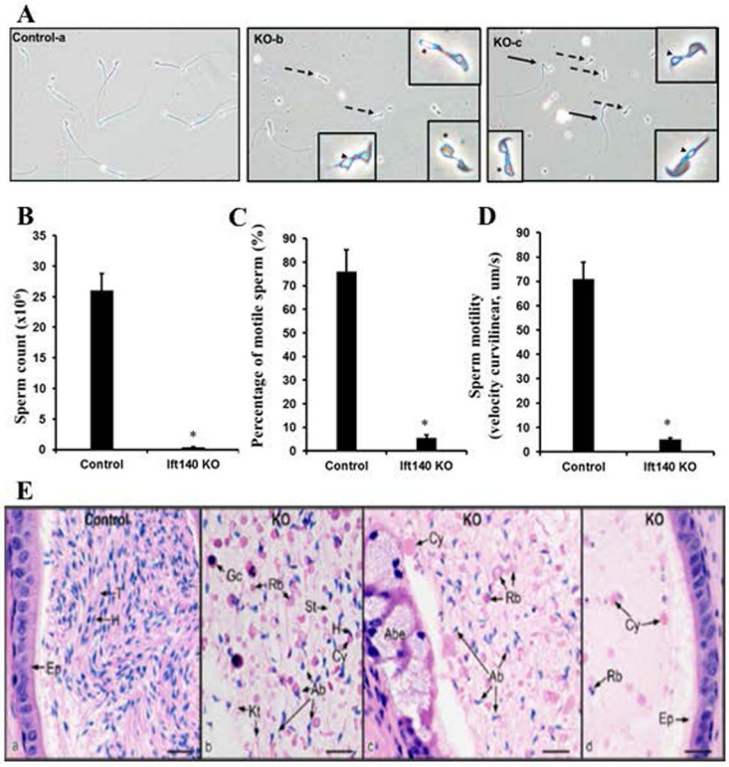

Figure 3. Disruption of *Ift140* in male germ cells results in abnormal sperm morphology, reduced sperm number and mobility

A. Morphological examination of cauda epididymal sperm collected from 3~4-month-old control (a) and conditional *Ift140* KO mice (b–c) by light microscopy. Notice that compared to the control, much cell debris and very few sperms were observed in the conditional *Ift140* KO mice under the same dilution. Sperms from the *Ift140*-deficient mice had bent (black arrows in c) or short tails (dashed arrows in b and c). Some sperms had swollen tail tip (asterisk in b and c). Vacuoles were present at the base of stunted flagella (arrowheads in b and c). B. Sperm count is significantly reduced in the KO mice. C. Comparison of percentage of motile sperm between the control and *Ift140* KO mice. D. Analysis of sperm motility by calculating curvilinear velocity (VCL). Sperm VCL was largely decreased in the *Ift140*-deficient mice compared to the controls (* $p < 0.05$). **E.** Histology of the cauda epididymis from control (heterozygote) and conditional *Ift140* mutant mice (KO). (a) Control epididymis showing highly concentrated epididymal sperm with aligned sperm tails (T) and normal sperm heads (H). Ep, epithelium. (b) KO epididymal lumen showing abnormal sperm heads (Ab), cytoplasmic bodies with and without sperm heads (H), short tails (St), residual bodies (Rb), kinked tails (Kt) and sloughed germ cells (Gc). (c) KO epididymis showing an area of abnormal epithelium (Abe). The lumen contains abundance of large cytoplasmic bodies (Cy), residual bodies (Rb) and numerous abnormally shaped sperm heads (Ab). (d) KO epididymis with normal epithelium (Ep), but a lumen containing scattered cytoplasmic bodies (Cy) and residual bodies (Rb), with no sperm heads present. Bars = 20 μm.

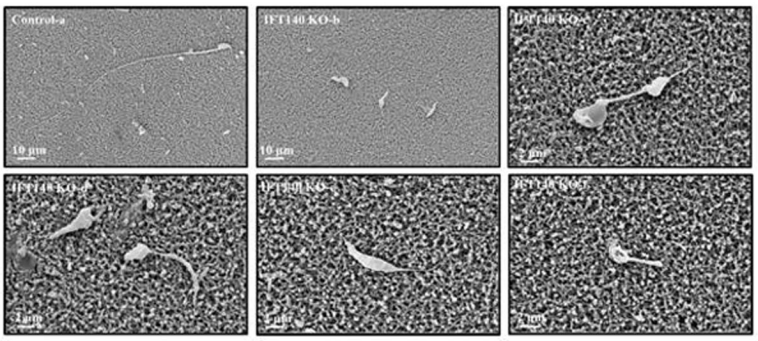

Figure 4. Examination of epididymal sperm by SEM

(a) Representative image of epididymis sperm with normal morphology from a control mouse shows the sperm with a long, smooth tail and condensed head. (b–f) Representative images of epididymal sperm from a conditional *Ift140*-deficient mouse. A variety of morphologic abnormalities of sperm were observed. The sperm displayed amorphous heads (d, e), short/swollen flagella (b to f), uneven thickness of flagella (d), and other distorted shapes.

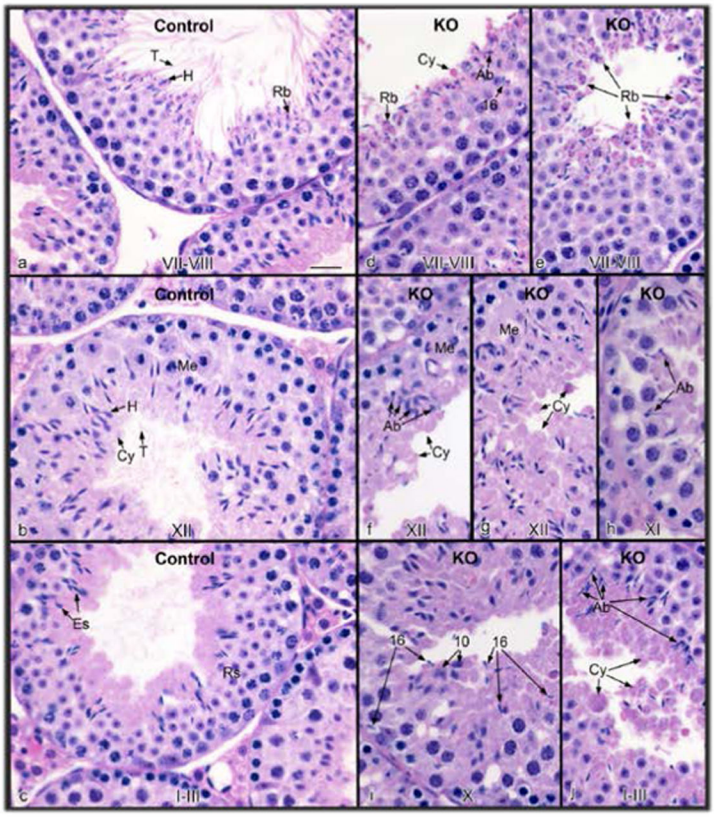

Figure 5. Histology of the testis from control (a–c) and conditional *Ift140* knockout (KO) mice (d–j)

The stage of spermatogenesis is identified at the bottom of each figure. (a) Control stage late VII–VIII, showing normal step 16 elongated spermatids with long tails (T) extending into the lumen and heads (H) surrounded by forming residual bodies (Rb). (b) Control stage XII, showing spermatocytes in meiotic division (Me), step 12 elongating spermatids with heads (H) of condensed chromatin, bulges of cytoplasm (Cy) and tails extended into the lumen. (c) Control stage I–III, showing elongated spermatids (Es) with tails extending into the lumen and heads extending toward the round spermatids (Rs). (d) KO stage VII–VIII, showing failure of spermiation of step 16 spermatids that were retained in the epithelium, and accumulation of residual bodies (Rb) and cytoplasmic bodies (Cy) at the lumen. Abnormally shaped spermatid heads (Ab) are also present. (e) KO stage VII–VIII, showing the release of residual bodies (Rb) into the lumen, with some attached spermatid heads. (f) KO stage XII, showing accumulation of abnormal spermatids (Ab), with cytoplasm (Cy) extending into the lumen without the formation of tails. Spermatocytes in meiotic division (Me) appear normal. (g) KO stage XII, showing excess spermatid cytoplasm (Cy) being released into the lumen. Me, meiotic division. (h) KO stage XI, showing abnormal (Ab) elongated spermatid heads. (i) KO stage X, showing step 16 elongated spermatids mixed among step 10 spermatids, due to failure of spermiation in stage VIII. (j) KO stage I–III, showing the accumulation of spermatid cytoplasm bodies in the lumen (Cy), with some attached spermatid heads. Abnormally shaped spermatid heads (Ab) are also found lining the lumen. Bar = 20 μm for all photos.

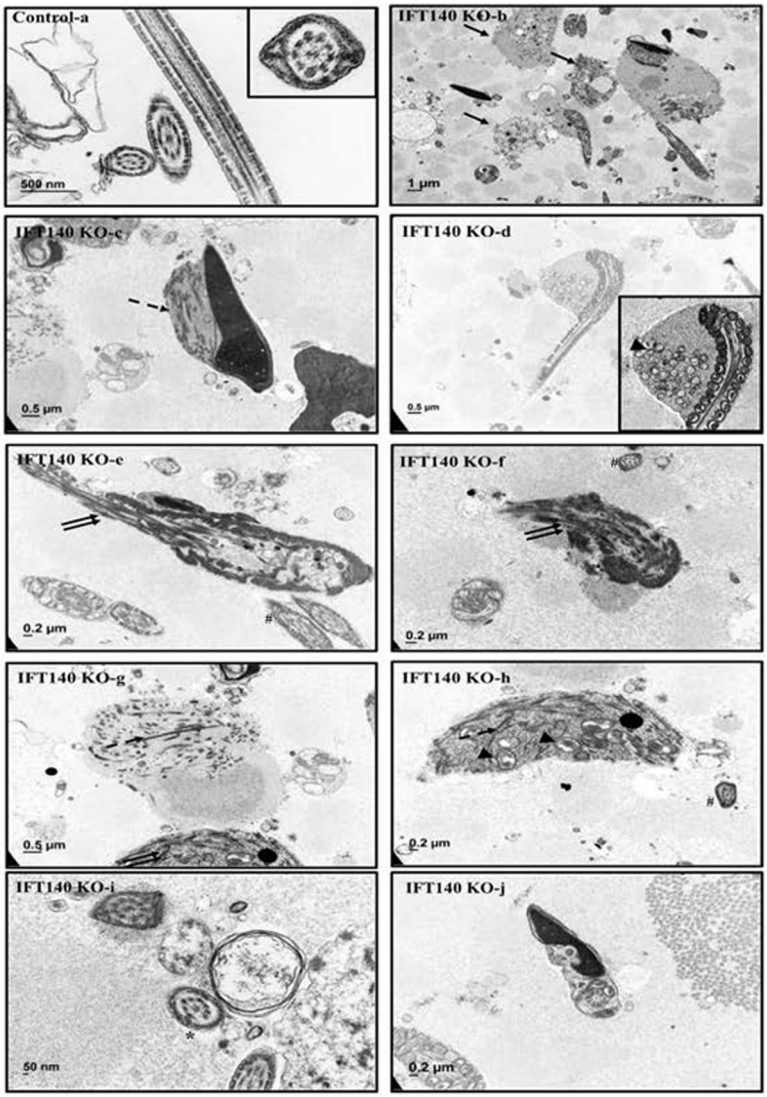

Figure 6. Analysis of epididymal sperm of the control and *Ift140* KO mice by TEM

TEM images of epididymal sperm from 4-month-old control and KO mice. Sperm from the control mice show normal ultrastructure (a). Few sperm were discovered in the collection from the KO mice. Instead, significant amounts of residual bodies (arrows in b) were present. The residual bodies and the very few sperm with redundant cytoplasmic components contained components for ODF and fibrous sheath (dashed arrow in c, g, h) and mitochondria (arrow head in d, h). Disorganized microtubule array (double arrows in e, f, g) were frequently seen. Some sperm lost “9+2” core axoneme structure (* in i); some have disorganized chromatin structure (j). Some sperm with apparently normal ultrastructure in cross-sections were still observed in the conditional Ift140 KO mice (# in e, f, h).

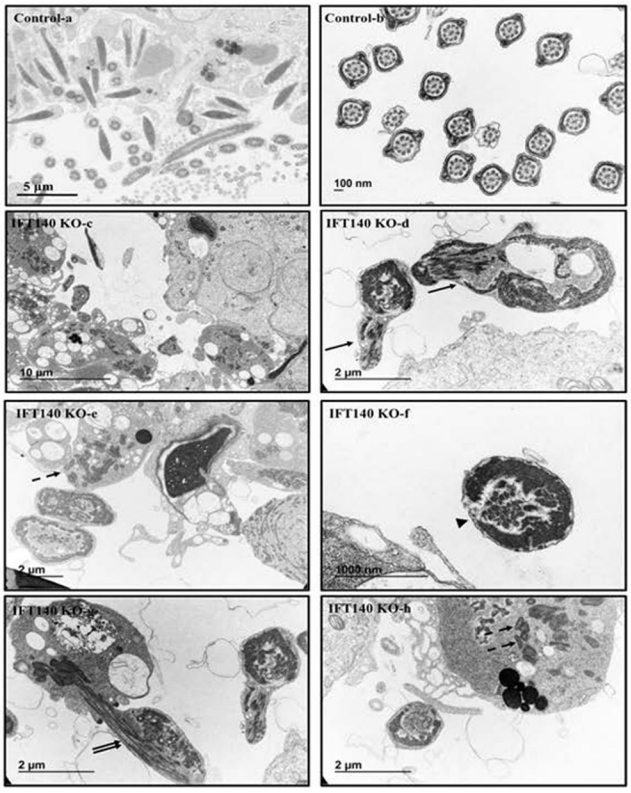

Figure 7. Analysis of testicular sperm of the control and *Ift140* KO mice by TEM

TEM images of testicular sperm from 4-month-old control and KO mice. In the control mice, sperm were easily discovered in the lumen of seminiferous tubules (a), and the ultrastructure was normal (b). However, few sperm were discovered in the KO (c), and the sperm usually have disorganized axoneme structure (arrows in d). The dashed-arrows in “e” and “h” point to the mitochondria materials in the residual bodies; the arrowhead in “f” points to an axoneme with disrupted “9+2” array; the double-arrows in “g” points to an axoneme with disorganized microtubules.

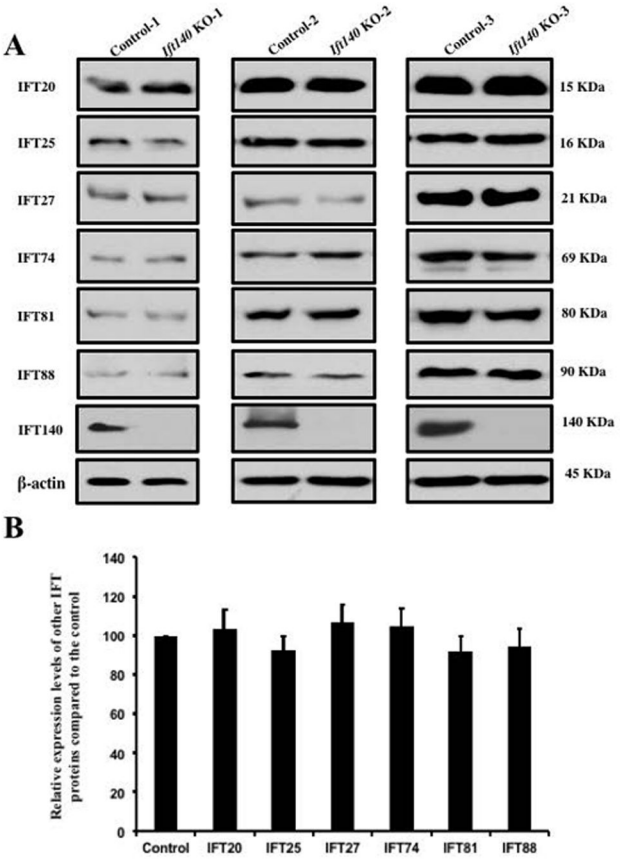

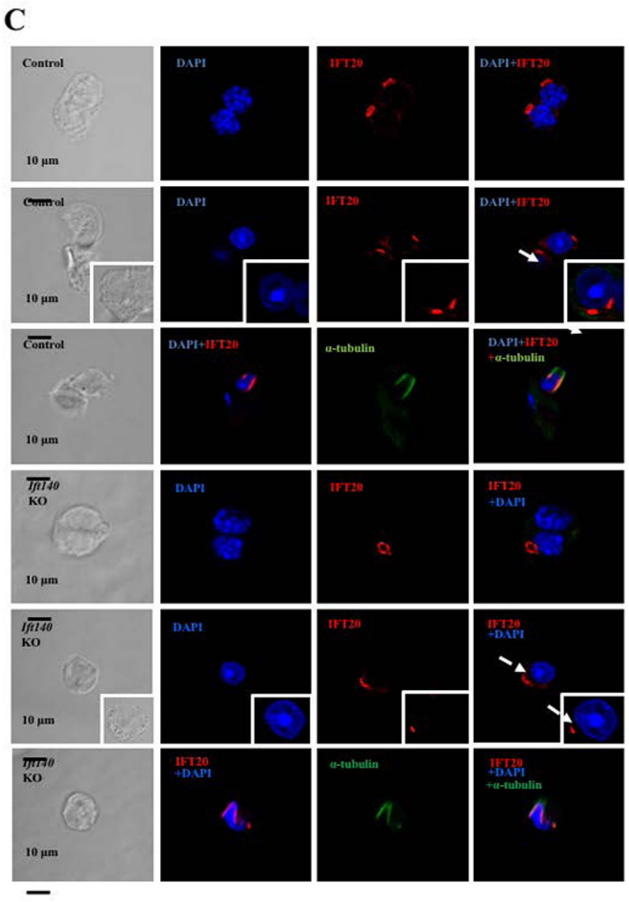

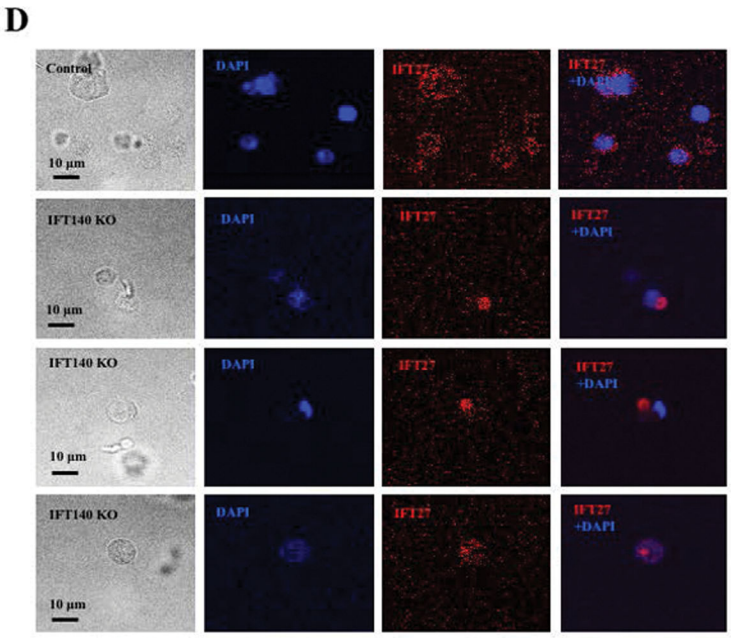

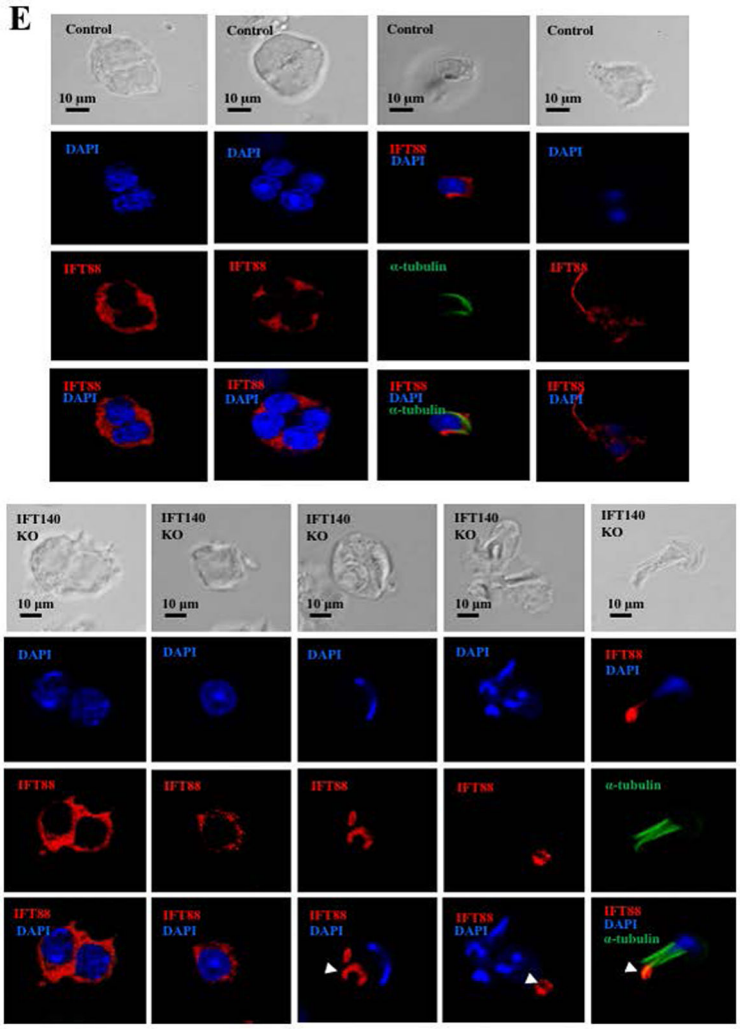

Figure 8. Expression of other IFT proteins in conditional *Ift140* KO mice

A. Representative Western blotting images showing testicular expression of IFT20, IFT25, IFT27, IFT74, IFT81, and IFT88 using specific antibodies in three control and three conditional *Ift140* mice. β-actin was used as a loading control. B. Statistical analysis of relative expression of the IFT proteins normalized by β-actin. There is no difference in expression levels of these selective IFT proteins between the controls and the *Ift140* KO mice. C. Localization of IFT20 in the germ cells of control and conditional *Ift140* knockout mice. In mice with both genotypes, IFT20 is present in the Golgi bodies of spermatocytes (upper panels), acrosome of round spermatids (middle panels), and manchette of elongating spermatids (lower panels). However, in the control animal, IFT20 appears to attach closely to the nuclear membrane (white arrow) in round spermatids; in the *Ift140* KO, IFT20 does not seem to attach tightly to the nuclear membrane (dashed white arrow). D. Abnormal localization of IFT27 in the conditional *Ift140* knockout mice. The granule-like pattern of the IFT27 signal was never observed in the control mice. E. Abnormal localization of IFT88 in the conditional *Ift140* knockout mice. In the control mouse, IFT88 is present in the cytoplasm of spermatocytes and round spermatids, manchette of elongating spermatids, and

the developing tails; In the *Ift140* KO mice, even though IFT88 is still present in the cytoplasm of spermatocytes and round spermatids, it accumulates abnormally in the germ cells at later stages (white arrow heads).

Table 1

Fertility, fecundity of control and conditional *Ift140* mutant mice

6 weeks old mice			Over 2-month old mice		
Genotype	**Fertility**	**Litter size**	**Genotype**	**Fertility**	**Litter size**
Control	10/10	9.3±2.3	Control	10/10	8.7±3.2
Ift140 KO	0/8	0	*Ift140* KO	0/8	0

To test fertility, adult and 6 weeks old males were bred to wild-type females for at least two months. Litter size was recorded for each mating.